The Performance of the GPSC/MSGC Hybrid Detector With Neon–Xenon Gas Mixtures

L. M. P. Fernandes, D. S. A. P. Freitas, A. M. F. Trindade, J. F. C. A. Veloso, C. M. B. Monteiro, L. F. Requicha Ferreira, and J. M. F. dos Santos

***Abstract*—The performance for X-ray spectrometry of neon–xenon gas proportional scintillation counters using a CsI-coated microstrip plate in direct contact with the scintillation gas as a VUV photosensor is investigated for different neon–xenon mixtures. At best operation conditions, the detector gain can reach values about 50% higher than those achieved with pure xenon filling. The highest gains and the best energy resolutions are achieved for xenon contents around 40%. However, the achieved energy resolutions are similar to those achieved with pure xenon. As in pure xenon and argon–xenon mixture gas fillings, the detector performance is limited by optical positive feedback resulting from additional scintillation produced in the electron avalanche processes around the MSP anodes. The best energy resolutions are achieved for positive feedback gains in the range of 1.1 to 1.2. The performance achieved with neon–xenon mixtures is inferior to that achieved with argon–xenon mixtures.**

***Index Terms*—CsI-photocathode, gas scintillation counter, microstrip gas chamber (MSGC), X-ray.**

I. Introduction

THE GAS proportional scintillation counter/microstrip gas chamber (GPSC/MSGC) hybrid detector has been developed recently [1], [2]. The photomultiplier tube (PMT) commonly used as the VUV photosensor in GPSCs is substituted in this detector by a CsI-coated microstrip plate (MSP), which is placed in direct contact with the GPSC filling gas, with the elimination of the GPSC scintillation window. Such hybrid detector presents an attractive alternative to PMT-instrumented GPSCs in applications where cost, compactness, detection-area, and power consumption are important. Additionally, integrated photosensors present a simple solution for operation at higher pressures than standard GPSCs [3].

Although the energy resolution achieved with a xenon GPSC/MSGC hybrid detector [11% full-width-at-half-maximum (FWHM) at 6 keV [3]] is not as good as that of PMT-based GPSCs (8% FWHM at 6 keV), the performance is already better than other xenon detectors based on charge avalanche amplification. The advantages in compactness, ruggedness, reduced power consumption, and insensitivity to operation under strong magnetic fields [4] are in themselves desirable attributes. The application of CsI-based photosensors operating in gaseous atmosphere is also being studied by other authors, e.g., [5], [6].

One of the factors limiting the performance of a xenon hybrid detector is the reduced number of photoelectrons that are transmitted to the avalanche region around the anode strips (being this 20%, 30%, and 50% of the photoelectrons emitted by the photocathode, at reduced electric fields above the cathode surface of 7, 20, and 36 $\mathrm{V \cdot cm^{-1} \cdot torr^{-1}}$, respectively, [7]). This is due to backscattering of the photoelectrons off the xenon atoms.

Other lower-Z filling gases, such as argon and neon, present more favorable photoelectron collection efficiency [7]–[9] (the ratio of the photoelectrons that escape from the photocathode to the number of emitted ones), which increases signal enhancement and improves the detector performance. Argon and argon–xenon hybrid detectors have been investigated [9], [10] and increased photoelectron collection efficiency in argon-based mixtures allowed a 50% increase in the detector gain, compared to that achieved with pure xenon [10].

Since photoelectron collection efficiency is higher for neon than for argon [7], [8], neon–xenon-based mixtures could improve the performance of the hybrid detector. On the other hand, the scintillation output of neon–xenon mixtures decreases with increasing neon content [11].

In this work, we present experimental results obtained with a GPSC/MSGC hybrid detector filled with different neon–xenon mixtures. The best experimental operation conditions, detector gain, and energy resolution will be investigated for each mixture.

II. Description

The GPSC/MSGC hybrid detector is depicted schematically in Fig. 1, being this the same detector as used in [1], [9], [10]. It features a 4-cm deep absorption/drift region and a 1-cm deep scintillation region separated by a mesh grid, G1 (80-μm diameter stainless-steel wire with 900-μm spacing). A Macor piece, glued with epoxy to the stainless-steel detector body and to the detector radiation window holder, is used for electrical insulation of the different electrodes. The stainless-steel support of G1 is fixed to the Macor with screws, one of which is used as a feedthrough for the G1-biasing voltage. The detector radiation window is a 50-μm Kapton film, aluminized on the inner surface, and glued with epoxy to its holder electrode. The upper and lower parts of the detector body are sealed by compression of a Viton o'ring.

Manuscript received November 13, 2003. This work was supported under projects POCTI/FIS/43527/00 and POCTI/FNU/49553/02, through Fundação para a Ciência e a Tecnologia (FCT and FEDER).

L. M. P. Fernandes, D. S. A. P. Freitas, A. M. F. Trindade, C. M. B. Monteiro, L. F. R. Ferreira, and J. M. F. dos Santos are with the Physics Department, University of Coimbra, P-3004-516 Coimbra, Portugal (e-mail: jmf@gian.fis.uc.pt).

J. F. C. A. Veloso is with the Physics Department, University of Coimbra, P-3004-516 Coimbra, Portugal, and also with the Physics Department, University of Aveiro, P-3810-193 Aveiro, Portugal.

Digital Object Identifier 10.1109/TNS.2004.832968

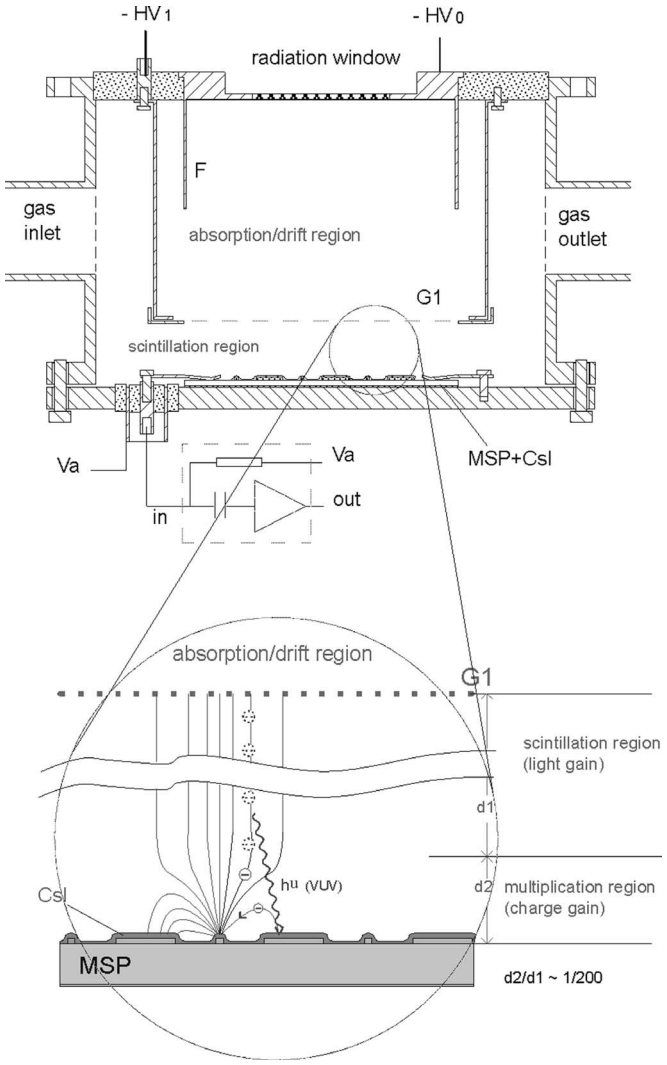

Fig. 1. Schematic of the GPSC/MSGC hybrid detector.

The MSP is the CERN model MS-4, consisting of 10-μm anodes and 80-μm cathodes with a 200-μm pitch, fabricated with 0.2-μm thick chromium film deposited on a 500-μm Desag D263 glass substrate. The backplane is a flat, unstructured layer of 0.1-μm chromium. A 500-nm thick and 30-mm in diameter layer of high-purity CsI was vacuum deposited onto the surface of the MSP. The presence of the CsI-coating does not compromise the operation of the MSP. On the other hand, it results in a reduced substrate charge built up, since its semiconductive characteristics are comparable to those of the semiconducting glass substrates used for high-rate MSP applications [12], [13].

The radiation window and the focusing electrode F are maintained at negative high voltage, $-\mathrm{HV}_0$, while grid G1 and its holder electrode are kept at $-\mathrm{HV}_1$. The MSP backplane and cathodes are maintained at ground potential, while a positive voltage V_a is applied to all the anodes. The electric field in the drift region is determined by the voltage difference between G1 and the radiation window, while the G1 voltage determines the electric field in the scintillation region. The anode-strips voltage determines the MSP gain.

The detector is filled with different neon–xenon mixtures at 800 torr (106 kPa), continuously purified by convection through nonevaporable getters at 150–200 °C. The ionizing radiation interacts in the absorption region and the resulting primary electron cloud drifts toward the scintillation region under the influence of a weak electric field (below the gas scintillation threshold). The electric field in the scintillation region is higher than in the absorption region, but lower than the gas ionization threshold, so that electrons can excite but not ionize the gas atoms. Upon crossing the scintillation region toward the MSP anode strips, each primary electron will produce a large number of VUV-photons, as a result of the gas de-excitation processes. The scintillation light intensity is proportional to the number of primary electrons and, thus, to the X-ray energy. The VUV scintillation photons, incident on the CsI-photocathode, induce the emission of photoelectrons from the active areas, the cathode strips. The photoelectrons drift toward the anode strips, producing charge avalanches in the intense electric field and, thus, a large signal proportional to the number of primary electrons produced by the X-rays in the gas.

A 2-mm collimated 5.9-keV X-ray beam from a ^{55}Fe radioactive source, with the 6.4-keV K_β line filtered with a chromium foil, was used to induce detector pulses. The anode pulses were pre-amplified with a CANBERRA 2006 charge-to-voltage preamplifier (sensitivity of 235 mV/10^6 ion pairs), linearly amplified with a TENNELEC TC243 amplifier (8-μs peaking time constants), and pulse-height analyzed with a 1024-multichannel analyzer. For peak amplitude and energy-resolution measurements, pulse-height distributions were fitted to a Gaussian superimposed on a linear background, from which the centroid and the FWHM were determined.

III. Experimental Results and Discussion

Fig. 2 presents typical pulse-height distributions obtained with the hybrid detector for a 2-mm collimated 5.9-keV X-ray beam and for different neon–xenon mixtures. In each case, the applied detector biasing voltages were those corresponding to the best performance. The spectral features include the 5.9-keV peak, the xenon L escape-peaks, and the electronic noise tail in the low-energy limit. The limit of the low-energy noise tail is around 600 eV for all mixtures, resulting in a signal-to-noise ratio of about 10 for 6 keV. The contribution of the electronic noise fluctuations to the energy resolution of the 6 keV is, thus, less than 1% FWHM absolute value.

In Fig. 3, we present the detector relative pulse amplitude as function of the MSP anode voltage V_a for the different neon–xenon mixtures, while maintaining the electric fields in the drift and scintillation regions constant. Exponential functions (solid lines) were superimposed on the experimental results, for comparison. The MSP-gain depicts the characteristic exponential variation of the charge avalanche processes at the MSP-anodes. However, for high V_a voltages, optical positive feedback, resulting from additional scintillation produced in the electron avalanche processes, results in a faster increase of the MSP-gain.

In Fig. 4, we depict the detector energy resolution and relative gain due to positive feedback, $\mathrm{G_{tot}}/\mathrm{G_{exp}}$ (where $\mathrm{G_{tot}}$ is the measured total gain of the detector and $\mathrm{G_{exp}}$ is the gain represented by the exponential function, Fig. 3) as function of V_a.

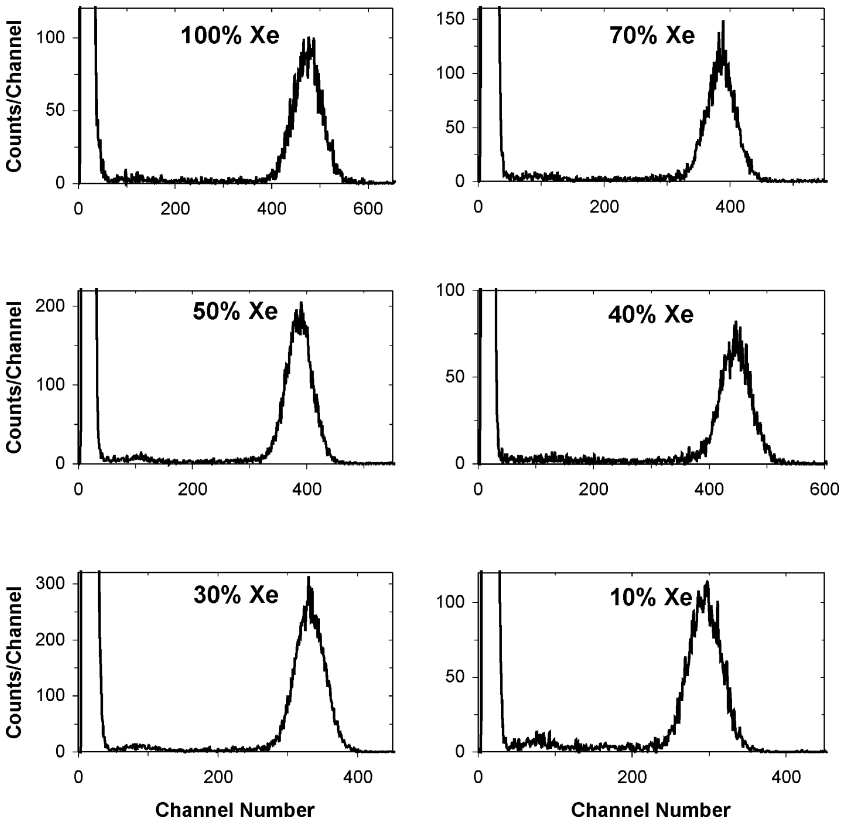

Fig. 2. Typical pulse-height distributions for 5.9-keV X-rays obtained with the GPSC/MSGC hybrid detector for different neon–xenon mixtures. The detector biasing voltages applied in each case correspond to those that deliver best performance.

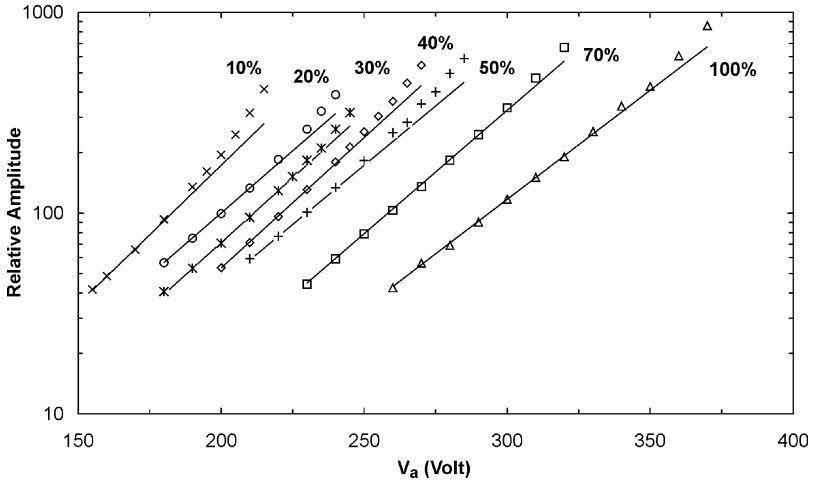

Fig. 3. Detector relative pulse amplitude as function of the anode-to-cathode strips voltage V_a for constant reduced electric fields in the drift and scintillation regions and for the different neon–xenon mixture-fillings. Exponential functions (solid lines) are superimposed to the experimental results, for comparison.

The solid lines serve only to guide the eye. As shown, the optical positive feedback limits the MSP maximum gain by limiting V_a, since positive feedback introduces additional statistical fluctuations that lead to a degradation of the detector energy resolution. On the other hand, the use of reduced V_a voltages at optimum operating conditions of the CsI-coated MSP has a benefit, since it results in negligible charge build up and prevents the possibility of MSP discharge breakdown.

As for argon–xenon mixtures, the detector energy resolution improves with the MSP-gain, degrading after the onset of the positive feedback effect. The best energy resolutions are achieved for positive feedback gains between 1.1 and 1.2, corresponding to V_a voltages around 205, 235, 245, 260, 270, 305, and 355 V for Ne-10% Xe, Ne-20% Xe, Ne-30% Xe, Ne-40% Xe, Ne-50% Xe, Ne-70% Xe, and pure xenon, respectively. These values are similar to those obtained for argon–xenon mixtures with the same xenon content, denoting the predominant role of xenon in the scintillation processes, in both cases.

The detector relative pulse amplitude and energy resolution were studied as a function of the reduced electric field E/p (the electric field intensity divided by the gas pressure p) in the scin-

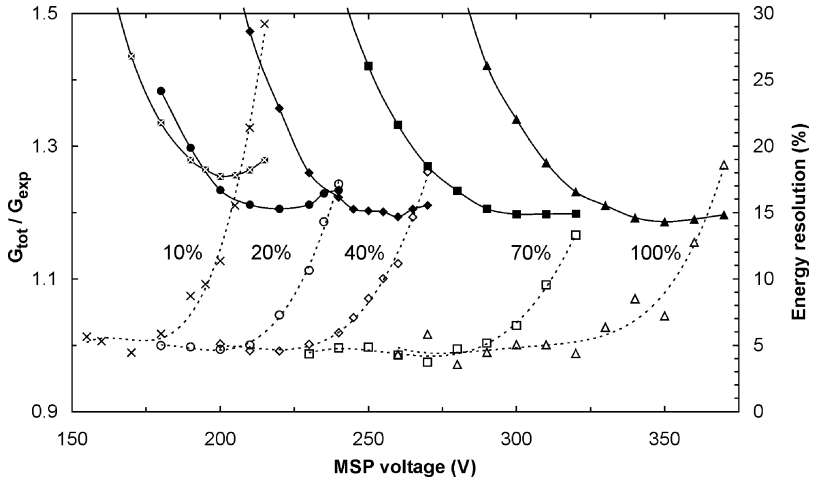

Fig. 4. (Open symbols) positive-feedback gain and (solid symbols) detector energy resolution, FWHM, as function of the anode-to-cathode strip voltages V_a for constant reduced electric fields in the drift and scintillation regions and for the different neon–xenon mixture-fillings. The solid lines serve only to guide the eye.

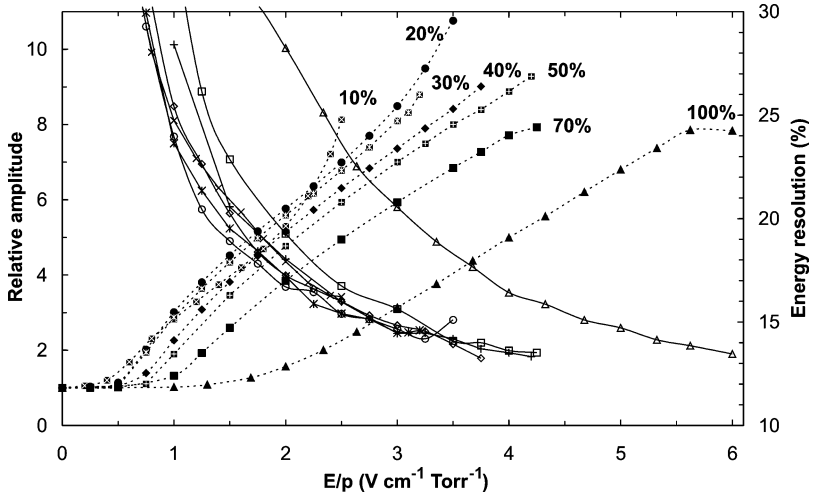

Fig. 5. (Open symbols) detector relative pulse amplitude and (solid symbols) energy resolution, FWHM, as function of the reduced electric field in the scintillation region for the different neon–xenon mixtures, using a constant photosensor-gain (at optimum value for each mixture) and a constant reduced electric field in the drift region. The solid curves serve only to guide the eye.

tillation region. However, the maximum achievable E/p was restrained due to insulation problems between the detector-body and the G1-holder and depended on the gas mixture.

Fig. 5 depicts the detector relative pulse amplitude and energy resolution as function of E/p in the scintillation region for the different neon–xenon mixtures, while keeping the reduced electric field in the drift region around 0.2 V cm$^{-1}\cdot$torr^{-1} (0.1 V$\cdot$cm$^{-1}\cdot$torr^{-1} for Ne-10% Xe) and the photosensor gain at its optimum value, for each mixture. The solid curves serve only to guide the eye.

The experimental results reveal the approximately linear trend, characteristic of the GPSC secondary scintillation yield. Below the gas scintillation-threshold, pulse-amplitudes become constant, the pulse height resulting only from the amplification of the primary electrons in the MSP-anodes. Above the gas ionization-threshold, the scintillation yield departs from the linear behavior, denoting a steeper increase due to the onset of charge avalanche multiplication in the scintillation region, as displayed in Ne-10% Xe and Ne-20% Xe data. According to [11], Table I, this departure will be observed at values of E/p of about 2.0, 2.5, 3.2, 3.8, 4.4, 5.5, and 7.0 V$\cdot$cm$^{-1}\cdot$torr^{-1}, for Ne-10% Xe, Ne-20% Xe, Ne-30% Xe, Ne-40% Xe, Ne-50% Xe, Ne-70% Xe, and pure xenon, respectively. However, for the hybrid detector, the detector gain tends to depart from this behavior at higher E/p values, and tends to saturate for pure xenon and high xenon content mixtures. This is due to the role of the electric field intensity, at the CsI surface, in the extraction of the produced photoelectrons, as discussed in [1], [9], and [10].

As shown in Fig. 5, the amplification achieved in the scintillation processes for neon–xenon mixtures is significantly higher than that obtained for pure xenon. Taking into account that the gas scintillation yield is almost independent of the xenon content, for E/p values above 3 V cm$^{-1}\cdot$torr^{-1} and below the onset of charge multiplication for each mixture (see Fig. 6 of [11]), the increase in gain confirms the improved photoelectron transmission expected for neon–xenon mixtures. The highest gains are achieved for xenon concentrations around 40%.

Extrapolating the results depicted in Fig. 5, for neon–xenon mixtures of 40% and 50%, to values of E/p in the

4 to 5 V $\cdot$ cm^{-1} $\cdot$ torr^{-1} region, the detector gain can reach values more than 80% to 70% higher than those obtained for pure xenon. These values compare favorably to those of 50% to 40%, achieved with argon–xenon mixtures (Fig. 5 of [10]), confirming the higher photoelectron transmission efficiency expected for neon–xenon mixtures compared to argon–xenon mixtures.

However, detector energy resolutions achieved with neon–xenon mixtures are similar to those obtained for pure xenon filling and somewhat poorer than those achieved with argon–xenon mixtures. This is due to the higher w values (i.e., the average energy to produce a primary electron) of neon–xenon mixtures, when compared to pure xenon and argon–xenon mixtures, which cancel out the benefits resulting from a higher photoelectron transmission.

Additionally, when compared to neon–xenon mixtures, argon–xenon mixtures achieve higher E/p values, prior to the onset of energy resolution degradation, resulting from the presence of charge multiplication in the scintillation region. Thus, with argon–xenon mixtures, it is possible to achieve similar or even higher scintillation gains with improved energy resolutions.

We note that the scintillation gains achieved in this work are around 25% to 30% inferior to those obtained in [10] (comparing the gains obtained for pure xenon of Fig. 5, in both works) and energy resolutions (FWHM) are degraded by about 1% absolute value. We attribute this difference to a degradation of the CsI-photocathode quantum efficiency, occurred during the time elapsed between the two works. However, this effect does not invalidate the results obtained for the relative behavior of the different gas mixtures.

IV. Conclusion

GPSC/MSGC hybrid detectors filled with neon–xenon mixtures present higher scintillation gains when compared to those filled with pure xenon and argon–xenon mixtures. At E/p values in the 4 to 5 V $\cdot$ cm^{-1} $\cdot$ torr^{-1} region, the detector gain can reach values more than 80% higher than those achieved with pure xenon filling. Nevertheless, energy resolutions are similar to those obtained with pure xenon. The highest gains and best energy resolutions are achieved for xenon concentrations around 40%.

Additionally, neon–xenon mixtures attain lower E/p values prior to the onset of energy resolution degradation, resulting from the presence of charge multiplication in the scintillation region, when compared to pure xenon and argon–xenon mixtures. Thus, argon–xenon mixtures may achieve similar or even higher scintillation gains with improved energy resolutions than neon–xenon mixtures.

As for pure xenon and argon–xenon gas fillings, the detector performance is limited by optical positive-feedback resulting from additional scintillation produced in the electron avalanche processes around the MSP anodes, limiting the MSP-gain for optimum operating conditions. The best energy resolutions are achieved for positive-feedback gains in the range of 1.1 to 1.2.

Acknowledgment

The authors would like to thank the Atomic and Nuclear Instrumentation Group of the Instrumentation Centre (Unit 217/94) of Departamento de Física, Universidade de Coimbra, where this work was carried out.

References

[1] J. F. C. A. Veloso, J. M. F. dos Santos, and C. A. N. Conde, "Gas proportional scintillation counter with a CsI-covered microstrip plate UV photosensor for high resolution X-ray spectrometry," *Nucl. Instrum. Methods A*, vol. 457, pp. 253–261, 2001.

[2] D. S. A. P. Freitas, J. F. C. A. Veloso, C. M. B. Monteiro, J. M. F. dos Santos, and C. A. N. Conde, "The gas proportional scintillation counter/microstrip gas chamber hybrid detector," *Nucl. Instrum. Methods A*, vol. 505, pp. 228–232, 2003.

[3] D. S. Covita, J. F. C. A. Veloso, F. D. Amaro, J. M. F. dos Santos, and C. A. N. Conde, "High-pressure xenon GPSC/MSGC hybrid detector," *IEEE Trans. Nucl. Sci.*, vol. 50, pp. 855–858, June 2003.

[4] J. F. C. A. Veloso, J. M. F. dos Santos, C. A. N. Conde, F. Mulhauser, P. Knowles, C. Donche-Gay, O. Huot, D. Taqqu, and F. Kottmann, "Driftless gas proportional scintillation counter for muonic hydrogen X-ray spectroscopy under strong magnetic fields," *Nucl. Instrum. Methods A*, vol. 460, pp. 297–305, 2001.

[5] D. Mormann, M. Balcerzyk, A. Breskin, R. Chechik, B. K. Singh, and A. Buzulutskov, "GEM-based gaseous photomultipliers for UV and visible photon imaging," *Nucl. Instrum. Methods A*, vol. 504, pp. 93–98, 2003.

[6] L. Periali, V. Peskov, P. Carlson, C. Iacobeause, T. Frankle, N. Pavlopoulos, P. Pichi, and F. Pietropaolo, "Evaluation of various planar gaseous detectors with CsI photocathodes for the detection of primary scintillation light from noble gases," *Nucl. Instrum. Methods A*, vol. 497, pp. 242–248, 2003.

[7] P. J. B. M. Rachinhas, J. A. M. Lopes, T. H. V. T. Dias, F. P. Santos, C. A. N. Conde, and A. D. Stauffer, "Photoelectron collection efficiency in rare gases: a Monte Carlo study," in *Proc. Int. Conf. Advanced Monte Carlo for Radiation Physics, Particle Simulation, and Applications*, Lisbon, Portugal, Oct., 2000, pp. 535–542.

[8] A. Di Mauro, E. Nappi, F. Posa, A. Breskin, A. Buzulutskov, R. Chechik, S. F. Biaggi, G. Paic, and F. Piuz, "Photoelectron backscattering effects in photoemission from CsI into gas media," *Nucl. Instrum. Methods A*, vol. 371, pp. 137–142, 1996.

[9] C. M. B. Monteiro, J. F. C. A. Veloso, D. S. A. P. Freitas, J. M. F. dos Santos, and C. A. N. Conde, "The gas proportional scintillation counter/microstrip gas chamber hybrid detector with argon filling," *Nucl. Instrum. Methods A*, vol. 490, pp. 169–176, 2002.

[10] C. M. B. Monteiro, J. F. C. A. Veloso, J. M. F. dos Santos, and C. A. N. Conde, "The performance of the GPSC/MSGC hybrid detector with argon–xenon gas mixtures," *IEEE Trans. Nucl. Sci.*, vol. 49, pp. 907–911, June 2002.

[11] T. H. V. T. Dias, F. P. Santos, P. J. B. M. Rachinhas, F. I. G. M. Borges, J. M. F. dos Santos, C. A. N. Conde, and A. D. Stauffer, "Xenonneon gas proportional scintillation counters: experimental and simulation results," *J. Appl. Phys.*, vol. 85, pp. 6303–6312, 1999.

[12] J. Va'vra, A. Breskin, A. Buzulutskov, R. Chechik, and E. Shefer, "Study of CsI photocathodes: volume resistivity and ageing," *Nucl. Instrum. Methods A*, vol. 387, pp. 154–162, 1997.

[13] R. Bouclier, M. Capeans, G. Million, L. Ropelewski, F. Sauli, T. Temmel, G. Della Mea, G. Maggioni, and V. Rigato, "High rate operation of micro-strip gas chambers on diamond-coated glass," *Nucl. Instrum. Methods A*, vol. 369, pp. 328–331, 1996.